

Dictionary-free Koopman model predictive control with nonlinear input transformation

Vít Cibulka^{1,2}, Milan Korda^{1,2}, and Tomáš Haniš¹

¹Department of Control Engineering, Faculty of Electrical Engineering, Czech Technical University in Prague, The Czech Republic

vit.cibulka@fel.cvut.cz, tomas.hanis@fel.cvut.cz

²CNRS, Laboratory for Analysis and Architecture of Systems, Toulouse, France
korda@laas.fr

December 29, 2022

Abstract

This paper introduces a method for data-driven control based on the Koopman operator model predictive control. Unlike existing approaches, the method does not require a dictionary and incorporates a nonlinear input transformation, thereby allowing for more accurate predictions with less ad hoc tuning. In addition to this, the method allows for input quantization and exploits symmetries, thereby reducing computational cost, both offline and online. Importantly, the method retains convexity of the optimization problem solved within the model predictive control online. Numerical examples demonstrate superior performance compared to existing methods as well as the capacity to learn discontinuous lifting functions.

1 Introduction

The Koopman operator approach is a successful framework for data-driven analysis of nonlinear dynamical systems that originated in the 1930s in the seminal works [1, 2] but gained wider popularity only much later in the mid 2000s with the advent of modern-day computing, starting with the works [3, 4]. The core idea is to represent the nonlinear system by an infinite-dimensional linear operator acting on the space of functions defined on the state-space (referred to as observables). Finite-dimensional approximations of this operator, computable from data using simple linear algebraic tools, then allow one to gain insight into the underlying dynamics and construct reduced-order models. This approach can be thought of as lifting of the original nonlinear dynamics into a higher dimensional space where it admits a linear description.

Generalizing this concept to control systems is far from trivial. A promising approach proposed in [5] defined the Koopman operator with control as acting on the product of the state-space and the space of all control sequences and used finite-dimensional approximations of this operator within a linear model predictive control scheme, nowadays referred to as the Koopman MPC. The primary

*This work has been supported by the Czech Science Foundation (GACR) under contract No. 20-11626Y, and by the Grant Agency of the Czech Technical University in Prague, grant No. SGS22/166/OHK3/3T/13. This work has also been supported by the AI Interdisciplinary Institute ANITI funding, through the French “Investing for the Future PIA3” program under the Grant agreement n° ANR-19-PI3A-0004 as well as by the National Research Foundation, Prime Minister’s Office, Singapore, under its Campus for Research Excellence and Technological Enterprise (CREATE) programme.

benefit is the convexity of the MPC problem solved online with computational complexity compared to classical linear MPC. The primary drawback is the inherent limitation of prediction accuracy. Indeed, the predictors proposed in [5] lift only the state whereas the control input remains untransformed and enters linearly into the predictor used within the MPC in order to preserve convexity. Therefore, fixing an initial condition, the mapping from the control input sequence to the output of the predictor is linear whereas the true mapping realized by the nonlinear system is typically nonlinear. A possible remedy is to consider bilinear predictors, which has a long history related to generalizing the classical Carleman linearization [6] to a controlled setting; see, e.g., [7, 8, 9, 10]. This, however, necessarily spoils the convexity of the MPC problem and is not pursued in this work. We refer the reader to the survey [11] for further discussion regarding the use of the Koopman operator in control.

A second drawback, common in controlled and uncontrolled settings, is the need for a user-specified dictionary of nonlinear lifting functions. Although such dictionaries may be naturally available for measure-preserving ergodic systems in the form of time-delayed measurements of the state [12], no such choice is available in more general settings and hence past works resorted to ad-hoc dictionaries (e.g., [13, 5]) such as radial basis functions or monomials. Even though efforts have been made to alleviate this by using a general parametrization of the dictionary (e.g., with neural networks [14]) or by exploiting the dynamics and state-space geometry to construct them [15], the need for a significant engineering effort in the design process has not been eliminated.

This work addresses the two principal issues described above as well as demonstrates how input quantization and symmetries of the problem can be exploited. Specifically, we first propose a class of predictors with nonlinear input transformation that preserves convexity of the MPC problem solved online and greatly improves the long-term prediction accuracy. To the best of our knowledge this is the first time that a nonlinear input transformation is employed while preserving convexity of the MPC problem.

Second, we eliminate the need for a dictionary by treating the values of the lifting functions on the available data samples as optimization variables in the (offline) learning process. Concurrently with our work, a different dictionary-free method for construction of Koopman predictors was developed in [16] using hidden Markov models; however, albeit providing accurate predictions, the models constructed therein are bilinear and hence lead to nonconvex problems when used within MPC.

In addition to this, we allow for input quantization, thereby bringing the method closer to practical applications where the control input is typically quantized.

Finally, we exploit symmetries in designing the predictors, thereby allowing for a more parsimonious parametrization of the predictors and hence faster learning; this could be seen as a generalization of the symmetry-exploitation methods without control proposed in [17] to the controlled setting where the interplay between state-space and control-space symmetries must carefully taken into account.

We demonstrate the effectiveness of our approach on several examples, including the highly nonlinear vehicle model adopted from our previous work in [18]. The current research around the Koopman operator for vehicle control includes [19] and [20], which both use the method [5] and therefore require user-specified dictionary for the state lifting. Another work is the already-mentioned [18], which did not require an explicit dictionary of lifting functions [15], but it still involved a notable engineering effort to construct the state lifting. Our paper uses the same vehicle model as [18], while minimizing the effort to construct the state lifting and, for the first time, employs input lifting. The proposed Koopman MPC significantly outperforms the previous methods on this vehicle model and, interestingly, the analysis of the input lifting functions unveils certain physical properties that can be directly tied to the vehicle dynamics.

Structure of this paper The Section 2 provides the problem statement and the Section 3 presents the main result of this paper. Then we discuss symmetry exploitations in the Section 4. Various implementation details of the method are presented in Section 5. The usage of the Koopman operator in control is presented in the Section 6, and the concrete form of the Koopman MPC used in this paper is summarized in the Section 7. The numerical examples are presented in the Section

8 and we conclude in the Section 9.

Notation All vectors are assumed to be column vectors. Set of integers from 1 to a will be denoted as $\mathbb{Z}_{1,a}$. The square of quadratic form $\sqrt{x^\top Q x}$ is denoted as $\|x\|_Q$. Cardinality of a set A is denoted as $|A|$. Identity matrix of size s is I_s , column vector of ones of size s is denoted as $\mathbf{1}_s$. Element-wise multiplication is denoted as \odot . A block-diagonal matrix with vectors a, b, c on the diagonal is denoted as $\text{bdiag}(a, b, c)$.

2 Problem statement

Let us consider a discrete controlled nonlinear dynamical system

$$\begin{aligned} x_{t+1} &= f(x_t, u_t) \\ y_t &= g(x_t), \end{aligned} \tag{1}$$

where $x_t \in X \subset \mathbb{R}^{n_x}$, $u_t \in U \subset \mathbb{R}^{n_u}$, $y_t \in Y \subset \mathbb{R}^{n_y}$ are the state, the input, and the output vectors.

We define the Koopman operator \mathcal{K} with control input as

$$\left(\mathcal{K} \begin{bmatrix} \Phi \\ \Psi \end{bmatrix} \right) \left(\begin{bmatrix} x \\ u \end{bmatrix} \right) = \Phi(f(x, u)), \tag{2}$$

where \mathcal{K} is the Koopman operator, $\Phi : X \rightarrow Z$ is the state lifting function, $\Psi : U \rightarrow V$ is the input transformation. The spaces Z and V are the Koopman state and input spaces respectively.

Note that the domain and codomain of the operator do not have the same dimension. This is because we consider controlled nonlinear dynamics, unlike the usual definitions which are for autonomous systems only. We do this because in this work we are not interested in the spectral properties of the operator; our goal is linear prediction of the controlled nonlinear dynamics (1).

The Koopman operator \mathcal{K} is generally infinite-dimensional and its usage is then numerically intractable from the very beginning. For this reason, we work only with its finite-dimensional approximation in the form of a linear-time-invariant (LTI) system.

The operator shall be approximated by a linear dynamical system as

$$\begin{aligned} z_{t+1} &= A z_t + B v_t \\ \hat{y}_t &= C z_t, \quad \text{for } z_0 = \Phi(x_0) \text{ and } v_t = \Psi(u_t), \end{aligned} \tag{3}$$

where $A \in \mathbb{R}^{n_z \times n_z}$, $B \in \mathbb{R}^{n_z \times n_v}$, $C \in \mathbb{R}^{n_y \times n_z}$ are matrices to be determined. The system (3) is referred to as the *Koopman predictor*; the state z_t is referred to as the *lifted state* and \hat{y}_t is the predicted output of the system (1).

The primary goal of this work is to find A, B, C, Ψ, Φ , such that the resulting LTI system (3) predicts the behaviour of the nonlinear dynamics (1) on X for H_T steps ahead. This predictor is then used for controller synthesis within Koopman MPC, which we describe in Section 6.

3 Finding the Koopman predictor

In this section we present a method for determining the Koopman predictor (3). We start by giving an intuition: Assuming that we have trajectory data (y_t, u_t, x_0) , we want to find the linear system (3) so that its output \hat{y}_t matches the trajectory data \hat{y}_t . The distinguishing feature of our work is that we do so in a *dictionary-free* manner, that is, by optimizing the values of Φ and Ψ on the available data without having to specify a dictionary of basis functions parametrizing Φ and Ψ . In addition to optimizing the values of Φ and Ψ , we also optimize over the system matrices A, B, C . See Figure 1 for an illustration.

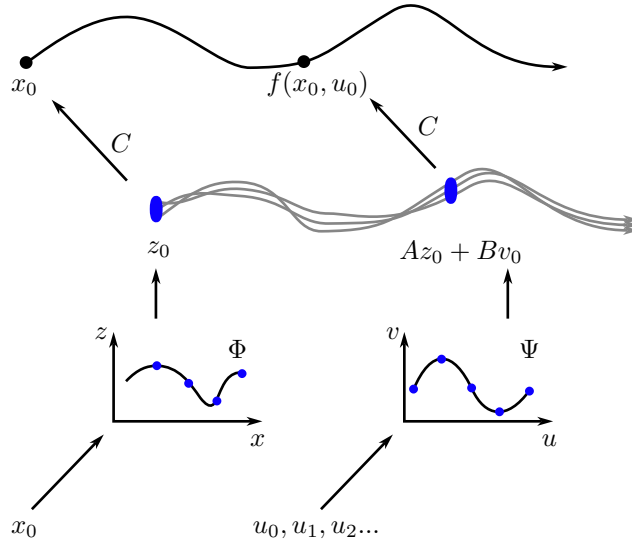


Figure 1: The approach behind the Koopman predictor with control. Both the initial state and the inputs are lifted via the functions Φ and Ψ respectively. The linearly evolving high-dimensional trajectory of the Koopman predictor (3) can then be projected onto the original state space, giving us the nonlinear trajectory of (1). The quantities optimized in our approach are highlighted in blue; this includes the values of Φ and Ψ on the available data.

Basic definitions

The optimization will be done over N trajectories of the real system (1), where the trajectories are chosen so that the output set Y is covered with a sufficient density. For this we first need to define the sets of initial conditions and admissible system inputs.

We will assume to have samples x_0^i from X , which are the initial states of the aforementioned trajectories of (1)

$$X_0 = \{x_0^i \in X : \forall i \in \mathbb{Z}_{1,N}\}. \quad (4)$$

To each $x_0^i \in X$, we associate a lifted initial condition $z_0^i \in Z_0 \subset \mathbb{R}^{n_z}$; these will be decision variables in the optimization problem where the control Koopman predictor is learned.

We will consider each input channel of the system (1) individually and assume that it is normalized. We also permit quantization of the control signal, thereby taking into account a digital control implementation or control signals that are discrete in nature (e.g., gears in a vehicle). The k^{th} input with q_k quantization levels reads

$$U_k \subset [-1, 1], \quad |U_k| = q_k. \quad (5)$$

The full input space can be retrieved by doing a cartesian product of the individual channels

$$U = U_1 \times U_2 \times \dots \times U_{n_u}. \quad (6)$$

In the optimization process, we will be searching for the transformed input channels V_k , which

have the same number of quantization levels as U_k :

$$V_k \subset [V_{k,\min}, V_{k,\max}], \quad |V_k| = q_k. \quad (7)$$

We do not make assumptions on the maxima and minima of the lifted input channels, since they are optimization variables.

After finding the Koopman predictor, we can retrieve the lifted input space as

$$V = V_1 \times V_2 \times \cdots \times V_{n_u}. \quad (8)$$

We will assume that the dimensions of both the original and lifted inputs are the same, i.e. $n_v = n_u$. Although this assumption is not required by the algorithm itself, the benefit of raising the input dimension is not investigated in this paper. The values V_k are initialized by the user. In this work, we initialize them by the values U_k as mentioned in the Table 1.

The Example 1 shows the advantage of considering the inputs channel-by-channel, instead of working with the whole cartesian product (6).

Example 1. Assume that we have two input channels quantized as

$$U_1 = \{-1, 1\}, U_2 = \{-1, 0.4, 1\}, \quad (9)$$

with $q_1 = 2$ and $q_2 = 3$. We retrieve U as

$$U = \left\{ \begin{bmatrix} -1 \\ -1 \end{bmatrix}, \begin{bmatrix} 1 \\ -1 \end{bmatrix}, \begin{bmatrix} -1 \\ 0.4 \end{bmatrix}, \begin{bmatrix} 1 \\ 0.4 \end{bmatrix}, \begin{bmatrix} -1 \\ 1 \end{bmatrix}, \begin{bmatrix} 1 \\ 1 \end{bmatrix} \right\}. \quad (10)$$

Optimizing over the channels V_1 and V_2 will introduce $\sum_k q_k = 5$ optimization variables. Should we, however, optimize over the whole set V , we would have $n_u \prod_k q_k = 12$ variables.

Considering each channel individually decreases the parameter space of the optimization and therefore increases the scalability of the algorithm. It also makes it easier to enforce invertibility of the transformation Ψ , which is crucial in control applications. This is discussed further in Section 6.2.4.

All the input vectors considered further in this section are elements of either U or V , and can be represented by a linear operator $\mathcal{L} : \mathbb{R}^{\sum_k q_k} \rightarrow \mathbb{R}^{n_u}$. Let us assume that we have an input $u' \in U$ and a corresponding lifted input $v' \in V$. We can write u' as

$$u' = \mathcal{L}'(U_1, U_2, \dots, U_{n_u}), \quad (11)$$

where \mathcal{L}' selects appropriate values from the channels U_k in order to build the vector u' . The same operator can be used for the lifted vector v' as

$$v' = \mathcal{L}'(V_1, V_2, \dots, V_{n_u}). \quad (12)$$

Action of a linear operator can be represented by matrix multiplication; we shall represent the operator \mathcal{L} by a matrix L . For u' we get

$$u' = L' [U_1^\top \quad U_2^\top \quad \dots \quad U_{n_u}^\top]^\top \quad (13)$$

and similarly for v' , with the same matrix L' . The matrix L (and L') is a block-diagonal matrix with row one-hot vectors on the diagonal, selecting only one element from each channel; it shall be referred to as *projection matrix*.

The Example 2 demonstrates the linear mapping via the projection matrix L .

Example 2. Assume $u' = [-1 \ 0.4]^\top$, $U_1 = \{-1, 1\}$, and $U_2 = \{-1, 0.4, 1\}$. The equation (13) would then look as

$$u' = L' \begin{bmatrix} U_1 \\ U_2 \end{bmatrix}$$

$$\begin{bmatrix} -1 \\ 0.4 \end{bmatrix} = \begin{bmatrix} 1 & 0 & 0 & 0 & 0 \\ 0 & 0 & 0 & 1 & 0 \end{bmatrix} \begin{bmatrix} -1 \\ 1 \\ -1 \\ 0.4 \\ 1 \end{bmatrix}, \quad (14)$$

therefore $L' = \text{bdiag}([1 \ 0], [0 \ 1 \ 0])$.

Assume that we have the lifted input channels defined as $V_1 = \{1, 0.2\}$, and $V_2 = \{4, 3, 0.1\}$. We can calculate the lifted vector v' which corresponds to u' by using the same matrix L' as

$$v' = L' \begin{bmatrix} V_1 \\ V_2 \end{bmatrix} = \begin{bmatrix} 1 & 0 & 0 & 0 & 0 \\ 0 & 0 & 0 & 1 & 0 \end{bmatrix} \begin{bmatrix} 1 \\ 0.2 \\ 4 \\ 3 \\ 0.1 \end{bmatrix} = \begin{bmatrix} 1 \\ 3 \end{bmatrix}. \quad (15)$$

The correspondence between u' and v' is therefore explicitly established by sharing the same projection matrix L' .

Finally, let us define the set of trajectories of the system (1) as \mathcal{T} . A single trajectory $\mathcal{T}_i \in \mathcal{T}$ with initial condition $x_0^i \in X_0$ and length H_T is defined as

$$\begin{aligned} \mathcal{T}_i &= \{(x_0^i, u_s^i, y_s^i) \in X \times U \times Y \\ &\text{s.t. } y_s^i = g(x_s), x_{s+1} = f(x_s, u_s^i) \\ &\forall s \in 0 \dots H_T - 1, \text{ for } x_0 = x_0^i \\ &\text{and } u_s^i = L_s^i [U_1^\top \ \dots \ U_{n_u}^\top]^\top\}, \end{aligned} \quad (16)$$

where H_T is the length of the trajectories, and L_s^i is a projection matrix associated with the input u_s^i . The dataset of multiple trajectories is denoted as $\mathcal{D} = \{\mathcal{T}_i \in \mathcal{T} : \forall i \in \mathbb{Z}_{1,N}\}$, where N is number of trajectories.

We will obtain the state lifting function $\Phi : \mathbb{R}^{n_z} \rightarrow \mathbb{R}^{n_x}$ by pairing the vectors x_0^i and z_0^i as

$$z_0^i = \Phi(x_0^i) \quad \forall i \in \mathbb{Z}_{1,N}, \quad (17)$$

where $z_0^i \in Z_0$ and $x_0^i \in X_0$.

Due to the channel separation, the input lifting function Ψ is built by concatenating individual functions $\Psi_k : \mathbb{R} \rightarrow \mathbb{R}$. The j^{th} element of the k^{th} channel input vector is transformed as

$$v_k^j = \Psi_k(u_k^j) \quad \forall j \in \mathbb{Z}_{1,q_k},$$

where $u_k^j \in U_k, v_k^j \in V_k$.

$$(18)$$

We can write $\Psi : \mathbb{R}^{n_u} \rightarrow \mathbb{R}^{n_u}$ as

$$\begin{bmatrix} v_1 \\ \vdots \\ v_{n_u} \end{bmatrix} = \begin{bmatrix} \Psi_1(u_1) \\ \vdots \\ \Psi_{n_u}(u_{n_u}) \end{bmatrix}. \quad (19)$$

With the definitions (17) and (19), optimizing over samples of Z_0 and V_k could be viewed as optimizing over the image of the lifting functions Φ and Ψ respectively.

3.1 Optimization problem setup

As a reminder, the output of the linear system (3) at time k for initial condition $z_0^i \in Z_0$ is

$$\hat{y}_t^i = C \left(A^t z_0^i + \sum_{j=0}^{t-1} A^{t-1-j} B v_j \right) \quad (20)$$

To find the Koopman predictor, we will seek to solve the problem

$$\begin{aligned} & \text{minimize } \sum_{i=0}^N \sum_{t=0}^{H_T} \|C z_t^i - y_t^i\|_2^2 + w_0 \sum_{(a,b) \in \mathcal{S}} \|z_{H_T}^a - z_0^b\|_2^2 + \theta(\cdot) \\ & \text{s.t. } z_t^i = \left(A^t z_0^i + \sum_{j=0}^{t-1} A^{t-1-j} B v_j^i \right) \\ & \quad v_j^i = L_j^i [V_1^\top \quad \dots \quad V_{n_u}^\top]^\top \end{aligned} \quad (21)$$

where A, B, C, z_0^i, V_k are the problem variables, $\mathcal{S}, L_j^i, y_t^i \in \mathcal{D}$ are the problem data, and H_T and N are the trajectory length and number of trajectories respectively. The scalar w_0 is a weighting parameter. The set \mathcal{S} contains indices of consecutive trajectories so for any $(a, b) \in \mathcal{S}$, \mathcal{T}_a ends at the same point where \mathcal{T}_b begins; the reasoning behind this regularization is explained further below, in 5.1.

The first term in the cost function ensures the fit of the data; the second one promotes invariance of Z_0 by connecting the consecutive trajectories in the lifted space, it can also be thought of as a regularization term. The last term, θ , is a placeholder for additional optional regularization which will be discussed in the section 5. The problem 21 can be simplified in terms of the number of variables and data requirements by exploiting symmetries of system 1, which will be discussed in the next section.

4 Exploiting symmetry

Assuming the nonlinear system (1) has a symmetry with respect to a symmetry group Γ , we can exploit this symmetry in our algorithm to decrease the size of the dataset by imposing a structure onto the matrices (A, B, C) , which will guarantee that the Koopman predictor will respect the same symmetries as (1). This means that the learning dataset \mathcal{D} will not need to contain symmetric trajectories, since the symmetry will be implicitly enforced by the structure of (A, B, C) , thus decreasing the size of \mathcal{D} , Z_0 , and the number of decision variables in (A, B, C) .

An action γ of the group Γ on vectors $x \in X$ and $u \in U$ are denoted as $\gamma^x x$ and $\gamma^u u$ respectively. The dynamical system is called Γ -equivariant with respect to the actions of Γ , if for all $x \in X$ and $\gamma \in \Gamma$

$$f(\gamma^x x, \gamma^u u) = \gamma^x f(x, u) \quad (22)$$

In this work, we shall assume only sign symmetries, meaning that the actions γ perform a sign-inversion of some of the components of their argument. The action γ^x is defined as a vector of size n_x containing n_Γ independent sign changes, $s_1, \dots, s_{n_\Gamma} \in \{-1, 1\}$, where $n_\Gamma \leq n_x$. For example $\gamma^x = [s_1 \quad s_2 \quad s_2 \quad s_3]_{n_x}^\top$. The action γ^u is a vector of size n_u and contains the same sign flips s_i but not necessarily all of them. For example $\gamma^u = [s_1 \quad s_2]^\top$. We shall slightly abuse the notation to denote $\gamma^x x = \text{Diag}(\gamma^x)x$ and $\gamma^u u = \text{Diag}(\gamma^u)u$.

The relation between γ^x and γ^u is determined by a matrix $H \in \mathbb{R}_+^{n_x \times n_u}$, such that

$$\gamma^x = \gamma_{\text{A}}^x + H\gamma^u, \quad (23)$$

where γ_{A}^x contains only elements of γ^x which are connected to uncontrollable states which respect some symmetry regardless of the inputs. Formally,

$$\gamma_{\text{A},i}^x = \begin{cases} 0, & \text{if } \gamma_i^x \in \gamma^u \\ \gamma_i^x, & \text{otherwise} \end{cases} \quad (24)$$

The matrix H is chosen such that its density is maximized. In other words, if we define the set of all matrices that fulfill (23) as $\mathcal{H} = \{\hat{H} : \gamma^x = \hat{H}\gamma^u\}$, we can obtain the matrix with the maximum density as

$$\bar{H} = \sum_{\hat{H} \in \mathcal{H}} \hat{H} \quad (25)$$

The matrix H is then obtained by row-normalizing \bar{H} as

$$H = \begin{bmatrix} H^1 \\ \vdots \\ H^{n_x} \end{bmatrix}, \text{ where } H^i = \begin{cases} \frac{\bar{H}^i}{\|\bar{H}^i\|_1}, & \text{if } \bar{H}^i \neq \mathbf{0}, \\ \mathbf{0}, & \text{otherwise.} \end{cases} \quad (26)$$

With this construction, i^{th} row of H has non-zero elements exactly at indices at which the vector γ^u has the same sign as γ_i^x

$$\gamma_p^u = \gamma_i^x \iff H_{i,p} \neq 0. \quad (27)$$

With the row normalization (26), we can also write

$$H^k \gamma^u = \sum_j H_{k,j} \gamma_j^u = \gamma_k^x \sum_j H_{k,j} = \gamma_k^x. \quad (28)$$

For example, assume the following discrete dynamical system $x^+ = f(x, u)$ (we drop the index k for readability):

$$\begin{aligned} x_1^+ &= -x_1 u_1 - |x_2| \\ x_2^+ &= -x_2 + u_2 + u_3 \\ x_3^+ &= -x_3 |x_2| + u_2 + u_3 \\ x_4^+ &= -x_4. \end{aligned} \quad (29)$$

The actions for this systems are defined as $\gamma^x = [s_1 \ s_2 \ s_2 \ s_3]$ and $\gamma^u = [s_1 \ s_2 \ s_2]$, where $[s_1 \ s_2 \ s_3] = [1 \ -1 \ -1]$, meaning that only the first state (and input) has no symmetry. We verify these actions by plugging them into (22)

$$\begin{aligned} f(\gamma^x x, \gamma^u u) &= \begin{bmatrix} -s_1^2 x_1 u_1 - |s_2 x_2| \\ -s_2 x_2 + s_2 u_2 + s_2 u_3 \\ -s_2 x_3 |s_2 x_2| + s_2 u_2 + s_2 u_3 \\ -s_3 x_4 \end{bmatrix} \\ &= \begin{bmatrix} s_1(-x_1 u_1 - |x_2|) \\ s_2(-x_2 + u_2 + u_3) \\ s_2(-x_3 |x_2| + u_2 + u_3) \\ s_3(-x_4) \end{bmatrix} = \gamma^x f(x, u) \end{aligned} \quad (30)$$

The matrix H and the vector γ_A^x are

$$H = \begin{bmatrix} 1 & 0 & 0 \\ 0 & 1/2 & 1/2 \\ 0 & 1/2 & 1/2 \\ 0 & 0 & 0 \end{bmatrix} \text{ and } \gamma_A^x = \begin{bmatrix} 0 \\ 0 \\ 0 \\ s_3 \end{bmatrix}, \quad (31)$$

which can be verified by direct application of (23)

$$H\gamma^u + \gamma_A^x = \begin{bmatrix} 1 & 0 & 0 \\ 0 & 1/2 & 1/2 \\ 0 & 1/2 & 1/2 \\ 0 & 0 & 0 \end{bmatrix} \begin{bmatrix} s_1 \\ s_2 \\ s_2 \end{bmatrix} + \begin{bmatrix} 0 \\ 0 \\ 0 \\ s_3 \end{bmatrix} = \begin{bmatrix} s_1 \\ s_2 \\ s_2 \\ s_3 \end{bmatrix} = \gamma^x. \quad (32)$$

In order to enforce the symmetry in the Koopman predictor, we need to define the action γ for the lifted vectors $z \in Z$ and $v \in V$. Since v has the same dimensions as u , and the transformation between them is done channel-wise, the action γ^v is equal to γ^u . For defining γ^z , we need to impose some structure onto the vector z . We do this by fixing the sparsity pattern of the C matrix to be able to explicitly link elements of z with concrete elements of x . The structure of the matrix C will be block-diagonal with $C = \text{bdiag}(c_1^\top, \dots, c_{n_x}^\top)$, where c_i are vectors of user-specified length. The i^{th} element of x can be then retrieved as

$$x^i = c_i^\top z^{c_i}, \quad (33)$$

where z^{c_i} is a part of the vector z which corresponds to c_i and has length $|c_i|$, the whole vector z can be written as $z = [z^{c_1^\top} \quad \dots \quad z^{c_{n_x}^\top}]^\top$.

Then we get

$$\begin{aligned} \gamma^x x &= \gamma^x C z = \gamma^x [c_1^\top z^{c_1} \quad \dots \quad c_i^\top z^{c_i} \quad \dots \quad c_{n_x}^\top z^{c_{n_x}}]^\top = \\ &[c_1^\top \gamma_{1,1}^x z^{c_1} \quad \dots \quad c_i^\top \gamma_{i,i}^x z^{c_i} \quad \dots \quad c_{n_x}^\top \gamma_{n_x,n_x}^x z^{c_{n_x}}]^\top = C \gamma^z z. \end{aligned} \quad (34)$$

Therefore

$$\gamma^z z = \begin{bmatrix} \gamma_1^x I_{|c_1|} & & \\ & \ddots & \\ & & \gamma_{n_x}^x I_{|c_{n_x}|} \end{bmatrix} \begin{bmatrix} z^{c_1} \\ \vdots \\ z^{c_{n_x}} \end{bmatrix}. \quad (35)$$

Finally, we can write

$$\gamma_k^z = \gamma_l^x \iff C_{l,k} \neq 0. \quad (36)$$

The matrix A will follow similar, block-diagonal, sparsity pattern with dense matrices on the diagonal

$$A = \text{bdiag}(A_{1,1}, \dots, A_{n_x,n_x}), \text{ where } A_{i,i} \in \mathbb{R}^{|c_i| \times |c_i|}. \quad (37)$$

The matrix B will have a sparsity pattern similar to the matrix H , except in vectorized form:

$$B = \begin{bmatrix} B^1 \\ \vdots \\ B^{n_x} \end{bmatrix}, B_{:,j}^i \in \begin{cases} \{0\}^{|c_i|} & \text{if } H_{i,j} = 0 \\ \mathbb{R}^{|c_i|} & \text{otherwise} \end{cases}, \quad (38)$$

where $B_{:,j}^i$ denotes the j^{th} column of the matrix B^i .

Lemma 1. *With the aforementioned definitions of γ^z , γ^v , and the sparsity patterns of A, B, C , the Koopman predictor respects the same symmetries as the nonlinear system, i.e. $A\gamma^z z + B\gamma^v v = \gamma^z(Az + Bv)$.*

Proof. Let us write (22) for the Koopman predictor:

$$\begin{aligned} A\gamma^z z + B\gamma^v v &= \gamma^z(Az + Bv) \\ A\gamma^z z + B\gamma^v v &= \gamma^z Az + \gamma^z(Bv). \end{aligned} \quad (39)$$

We get two equalities:

$$A\gamma^z z = \gamma^z(Az) \text{ and } B\gamma^v v = \gamma^z(Bv). \quad (40)$$

The first equality holds only if the matrices γ^z and A commute. Since γ^z is assumed to be block-diagonal, the matrix A also has to be block-diagonal matrix with the same block sizes.

Let us now show that the second equation

$$B\gamma^v v = \gamma^z(Bv) \quad (41)$$

holds as well with the aforementioned definitions.

Both side of the equation (41) are lifted vectors of size n_z , let us focus of its k^{th} element, which will be related to the l^{th} original state x_l via the C matrix, such that $C_{l,k} \neq 0$. The k^{th} element of (41) reads

$$\sum_j B_{k,j} \gamma_j^v v_j = \gamma_k^z \sum_j B_{k,j} v_j \quad (42)$$

Using (36), we get $\gamma_k^z = \gamma_l^x$

$$\sum_j B_{k,j} \gamma_j^v v_j = \gamma_l^x \sum_j B_{k,j} v_j \quad (43)$$

Now we use the fact that the row $B_{k,:}$ has the same sparsity pattern as $H_{l,:}$, from its definition in (38). Using the equation (27), we can write (43) as

$$B_{k,j} \neq 0 \iff H_{l,j} \neq 0 \quad (44)$$

and therefore

$$\gamma_j^u = \gamma_l^x \iff B_{k,j} \neq 0. \quad (45)$$

Now we can write the left side of (43) as

$$\sum_j B_{k,j} \gamma_j^v v_j = \gamma_l^x \sum_j B_{k,j} v_j \quad (46)$$

which concludes the proof and shows that the Koopman predictor will respect the symmetries of the nonlinear system, as long A, B , and C have the aforementioned sparsity patterns. \square

By fixing the sparsity patterns of the matrices A, B , and C , the Koopman system will respect the same symmetries as the nonlinear system. This will allow us to use less data for the training procedure. For example, assume that we know the lifted state $z_p \in Z$ is associated with $x_p \in X$, the lifted state of $\gamma^x x_p$ will be simply $\gamma^z z_p$; there is no need for including $\gamma^x x_p$ in the dataset, nor for having a separate variable for $\gamma^z z_p$.

5 Implementation details

This section describes certain details concerning the problem (21). First, we address the trajectory preparation in 5.1 and optional symmetry exploitation in 4. The solving of the problem (21) and its initialization are discussed in 5.2 and 5.3 respectively.

A summary of the whole process from data preparation to solving (21) is provided in 5.4.

5.1 Trajectory preparation

In order to improve the prediction capabilities and restrict overfitting, we force consecutive trajectories to have the same lifted values in their endpoints. This *endpoint consistency* is enforced by the term $\sum_{(a,b) \in \mathcal{S}} \|z_{H_T}^a - z_0^b\|_2^2$ of (21). The effect of (not) using it is shown in Fig.2. In our examples, we enforce the endpoint consistency and the prediction capabilities exceed the learning horizon H_T . This is shown in Fig.11 in the numerical examples section.

To make sure that our dataset contains consecutive trajectories, we generate long trajectories of length rH_T and split each into r trajectories of length H_T . Hence the final state of the first trajectory is the initial state of the second one and so on (only the last trajectories will have "free" final states). The indices of consecutive trajectories are stored in the set \mathcal{S} , as depicted in the Fig.3.

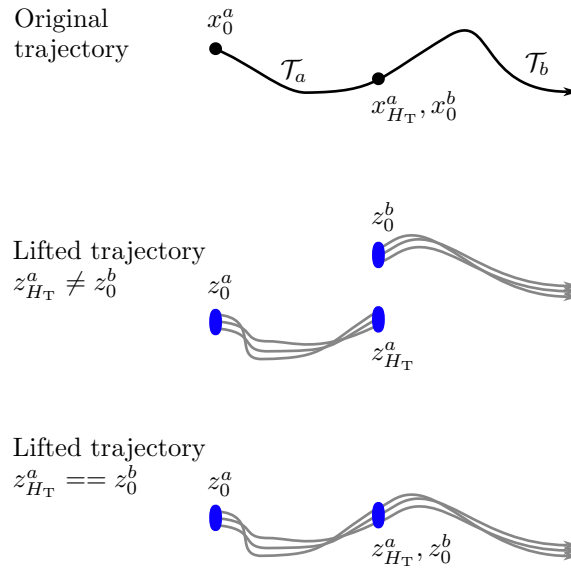


Figure 2: This figure demonstrates the effect of enforcing the endpoint consistency. Note that even when not enforcing it, we still obtain a valid predictor although the prediction capabilities will be strictly limited to the learning horizon H_T .

Since the problem (21) is very flexible in terms of variables, we need to make a clear distinction between controlled and autonomous trajectories, to prevent overfitting (we do not want controlled trajectory to be approximated by autonomous response and vice versa). For this, it is sufficient to start two trajectories from the same initial state, with different control inputs. This is also depicted in Fig.3. This is stated formally in the following Lemma.

Lemma 2. *Assume that we have two distinct trajectories of the nonlinear system (1), \mathcal{T}_i and \mathcal{T}_j , with $x_0^i = x_0^j$, $u_0^i \neq u_0^j$, and $y_1^i \neq y_1^j$. For any Koopman predictor \mathcal{K} , which approximates the trajectories with zero error, such that $z_0^i = z_0^j$, $z_0^i = \Phi(x_0^i)$, $z_0^j = \Phi(x_0^j)$, $Cz_1^i = y_1^i$, $Cz_1^j = y_1^j$, it holds that $\Psi(u_0^i) \neq \Psi(u_0^j)$.*

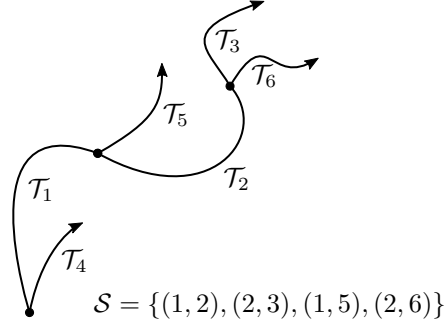


Figure 3: Example of trajectories used for learning and their interconnections. We see that one long trajectory was split into \mathcal{T}_1 , \mathcal{T}_2 , and \mathcal{T}_3 . The trajectories $\mathcal{T}_{4,5,6}$ start from the same initial conditions as $\mathcal{T}_{1,2,3}$ in this order. The set \mathcal{S} contains the indices of the interconnected trajectories.

Proof. Let us have two trajectories

$$\begin{aligned} \mathcal{T}_i &: (x_0^i, y_0^i, u_0^i), (y_1^i) \\ \mathcal{T}_j &: (x_0^j, y_0^j, u_0^j), (y_1^j) \end{aligned} \quad (47)$$

such that $i \neq j$, $u_0^i \neq u_0^j$, and $y_1^i \neq y_1^j$. We want to show that if $x_0^i = x_0^j$ then $\Psi(u_0^i) \neq \Psi(u_0^j)$.

Let us write the predictions of the Koopman predictor

$$\begin{aligned} \hat{y}_1^i &= C(Az_0^i + Bv_0^i) \\ \hat{y}_1^j &= C(Az_0^j + Bv_0^j), \end{aligned} \quad (48)$$

where $z_0^i = \Phi(x_0^i)$, $z_0^j = \Phi(x_0^j)$, $v_0^i = \Psi(u_0^i)$, $v_0^j = \Psi(u_0^j)$. By subtracting them, we obtain

$$\hat{y}_1^i - \hat{y}_1^j = CA(z_0^i - z_0^j) + CB(v_0^i - v_0^j). \quad (49)$$

Knowing that we have zero approximation error, we can write $\hat{y}_1^i = y_1^i$ and $\hat{y}_1^j = y_1^j$. Then by using the inequality $y_1^i \neq y_1^j$, we get

$$CA(z_0^i - z_0^j) + CB(v_0^i - v_0^j) \neq 0. \quad (50)$$

The inequality can be fulfilled by either the initial states or the inputs not being equal. However, if both trajectories start from the same initial condition, we get $z_0^i = z_0^j$ and the inequality can be only satisfied by $v_0^i \neq v_0^j$. \square

5.2 Solving the problem

The problem (21) can be formulated as a nonlinear unconstrained optimization problem after elimination of the linear equality constraints. It can be solved by a variety of solvers; in our case, we use the ADAM [21] optimization algorithm. ADAM is a first-order method for unconstrained problems, therefore it requires gradients of the cost function. We calculate the gradients of (21), via automatic differentiation (AD) routines, specifically by the packages Flux [22],[23] and Zygote [24] from Julia [25].

We would like to note that it seems beneficial to fix the values V_k during the first iterations of the ADAM solver. The lifted inputs will be more likely to retain the physical meaning of the original input variables. This is demonstrated in our last example in the Figures 12 and 13. In this paper, we fixed the input for the first 500 iterations.

5.3 Initialization values

The variables of (21) need to be initialized. Table 1 lists the choices used in this paper. We use $\mathcal{U}_{\alpha,\beta}$ to denote uniform distribution in the interval $[\alpha, \beta]$.

Variable	Initialization value(s)
z_0^i	Each element from $\mathcal{U}_{-1/2,1/2}$
V_k	Same as U_k
A	$a_{i,j} \in \mathcal{U}_{-1/2,1/2}$
B	$b_{i,j} \in \mathcal{U}_{-1/2,1/2}$
C	$c_{i,j} \in \mathcal{U}_{-1/2,1/2}$

Table 1: Initialization values for the problem (21).

It might be beneficial in some cases to initialize A such that its spectral radius is less than 1, which will make the initialized system (A, B, C) stable from a control-systems point of view.

5.4 Summary: Learning Koopman predictor

The algorithm 1 summarizes the procedure for learning the Koopman predictor.

Algorithm 1 Find the Koopman predictor (A, B, C, Φ, Ψ)

Input: f, g, X_0, H_T, q_k, N

- 1: Identify symmetries of the system f, g according to 4 and create the sparsity patterns for A, B, C .
- 2: Choose the number of quantization levels q_k and create the quantized channels U_k .
- 3: Generate N trajectories \mathcal{T}_i of length H_T according to 5.1
- 4: Initialize the matrices A, B, C , and the elements of Z_0 and V_k according to 5.3.
- 5: Solve (21), optionally fix the values V_k as mentioned in 5.2.

Output: A, B, C, Z_0, V_k

6 Koopman operator in control

In this section, we shall demonstrate the advantage of using a Koopman operator in control applications. More specifically, we will consider a Model Predictive Control (MPC) [26]. For a general nonlinear system (1), the MPC can be formulated as

$$\begin{aligned}
 J^* = \min \quad & \sum_{t=1}^H J_n(x_t) + J_c(x_t) \\
 \text{s.t.} \quad & x_{t+1} = f(x_t, u_t) \\
 & x_t \in X \\
 & u_t \in U,
 \end{aligned} \tag{51}$$

where J_c and J_n are convex and non-convex parts of the cost function in this order. This problem is non-convex due to the function J_n and the constraint $x_{t+1} = f(x_t, u_t)$; this makes the problem difficult to solve in general. We can, however, use the Koopman methodology to reformulate the problem in a convex fashion. We can eliminate the non-convex cost $J_n(x_t)$ by setting it as an additional output $\chi_t = J_n(x_t)$ and use the Koopman predictor of the form

$$\begin{aligned} z_{t+1} &= Az_t + Bv_t \\ \begin{bmatrix} \hat{\chi}_t \\ \hat{x}_t \end{bmatrix} &= Cz_t \\ z_0 &= \Phi(x_0), \end{aligned} \tag{52}$$

where $\hat{\chi}_t$ is an approximation of the non-convex cost $\chi_t = J_n(x_t)$. We can now rewrite (51) as

$$\begin{aligned} \hat{J}^* &= \min \sum_{t=1}^H \hat{\chi}_t + J_c(\hat{x}_t) \\ \text{s.t. } z_{t+1} &= Az_t + Bv_t \\ \begin{bmatrix} \hat{\chi}_t \\ \hat{x}_t \end{bmatrix} &= Cz_t \\ z_0 &= \Phi(x_0) \\ \hat{x}_t &\in X \\ v_t &\in V, \end{aligned} \tag{53}$$

where X is assumed to be convex and V is a box-constraint by construction (due to the channel-wise lifting). With these assumption in mind, the problem (53) is convex.

In a wide range of applications, the convex part of the cost is quadratic and the constraints are upper and lower bounds on some of the variables. This allows the user to formulate the problem (53) as a convex Quadratic Program (QP) – a well studied class of convex optimization problems with many solvers tailored to solving it efficiently such as ProxSuite [27], OSQP [28], and COSMO [29].

6.1 Koopman MPC

Let us exploit the benefits of the QP formulation and formulate our problem concretely, in a tracking form (minimizing the deviation of y_t from known y_{ref}) consistent with our own implementation used later in the Section 8. We shall refer to this optimization problem as Koopman MPC (KMPC):

$$\begin{aligned} \min_{\Delta v_t, z_t} \quad & \sum_{t=1}^H \|y_{\text{ref}} - Cz_t\|_Q^2 + \|v_t\|_R^2 + \|\Delta v_t\|_{R_d}^2 \\ \text{s.t. } \quad & z_{t+1} = Az_t + Bv_t \quad t = 1 \dots H - 1 \\ & v_t = \Delta v_t + v_{t-1} \quad t = 0 \dots H \\ & y_{\text{low}} \leq y_t \leq y_{\text{up}} \quad t = 1 \dots H \\ & v_{\text{low}} \leq v_t \leq v_{\text{up}} \quad t = 1 \dots H \\ & \Delta v_{\text{low}} \leq \Delta v_t \leq \Delta v_{\text{up}} \quad t = 1 \dots H \\ & z_0 = \Phi(x_0) \\ & v_0 = \Psi(u_{\text{prev}}), \end{aligned} \tag{54}$$

where $y_t = \begin{bmatrix} \hat{\chi}_t \\ \hat{x}_t \end{bmatrix}$, $Q \succcurlyeq 0$, $R \succ 0$, and $R_d \succ 0$. As mentioned before, this formulation solves the tracking problem where y_{ref} is an external parameter, and Δv_t is the optimization variable (instead

of v_t). The output, input, and input rate constraints are the pairs $(y_{\text{low}}, y_{\text{up}})$, $(v_{\text{low}}, v_{\text{up}})$, and $(\Delta v_{\text{low}}, \Delta v_{\text{up}})$ in this order.

The optimal solution is recovered as $u_t^* = \hat{\Psi}^{-1}(v_t^*)$, where $\hat{\Psi}$ is linearly interpolated version of Ψ . The problem is solved repeatedly at each time step, always using only the first control input u_1^* and then recalculating the solution from a new initial state. This approach provides closed-loop control and can be seen in Fig. 4.

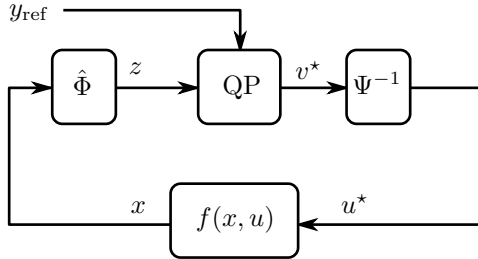


Figure 4: General MPC scheme using the Koopman operator as a control design model.

6.2 Practical considerations

For practical usage, we need to expand the domain of the lifting function Φ (17) to X , instead of X_0 . Another matter to consider is the invertibility of Ψ (19), since it is not guaranteed from (21).

Both of these matters are addressed in the following sections 6.2.3 and 6.2.4.

Regarding the connection of the Koopman predictor and MPC, we can expect the lifting functions to have a non-zero lifting error since we are working only with an approximation of the Koopman operator. The lifting error can be calculated and its knowledge exploited as a part of the MPC algorithm. This option is addressed in 6.2.1.

The last consideration is setting of the lifted input rate bounds $\Delta v_{\text{up/low}}$. These bounds do not naturally arise by finding the lifting functions (unlike $v_{\text{up/low}}$) and need to be set manually. We address this further in 6.2.2.

Lastly, we note that the problem (54) has the lifted state vectors z_t as variables. This greatly increases the total number of optimization variables since the dimension n_z may be large (recall that we are approximating infinite-dimensional operator). In the appendix, we show that the MPC can be formulated in a so-called condensed formulation, which has only Δv_t as variables, reducing the computational burden.

6.2.1 Lifting error

When the lifting via $\hat{\Phi}$ is not exact, we can use the knowledge of $\hat{\Phi}$ to calculate the lifting error at x_{init} and set it as output disturbance to the MPC to increase the precision of the calculation for the first timestep. The augmented output equation then reads

$$y_t = Cz_t + d_t, \quad (55)$$

where d is the initial-state lifting error

$$d_t = x_{\text{init}} - C\hat{\Phi}(x_{\text{init}}) \quad \forall t = 1, \dots, H. \quad (56)$$

This can be easily implemented by augmenting the state-space model as

$$\bar{A} = \begin{bmatrix} A & \\ & sI \end{bmatrix}, \bar{B} = \begin{bmatrix} B \\ 0 \end{bmatrix}, C = [C \quad I], \quad (57)$$

where $|s| \leq 1$ is the decay rate of d . Constant disturbance, considered in this work, is achieved by $s = 1$.

The error could be also estimated for the whole prediction horizon iteratively, by solving the QP multiple times and evaluating (56) for all the states x_t .

6.2.2 Input rate bounds

The bounds on Δv are not trivial to choose because the lifted-space bounds on v will not correspond to the real bounds on u because of the nonlinearity of Ψ , as seen in Fig.5. Possible solutions are

1. use the bounds with soft constraints to make them flexible
2. use ideas from nonlinear MPC and make an iterative scheme (and solve the QP multiple times)
3. use linearization of Ψ to set the bound
4. set the bounds on Δv conservatively, so that the worst case of Δu is guaranteed to be within its bounds.

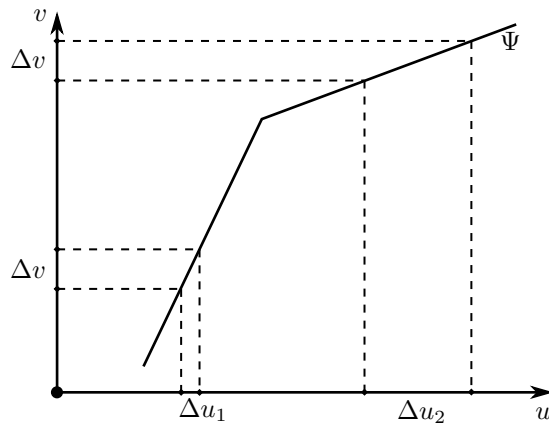


Figure 5: Example of a function Ψ , which would pose challenges with identifying desired bounds on Δv . We can see that the rate of u changes based on the slope of Ψ , even though the bound on Δv is constant.

6.2.3 Interpolation of Φ

As a result of the optimization process, we will obtain the samples of the function Φ in the form of pairs (x_0^i, z_0^i) , instead of the function itself. One needs to approximate $\hat{\Phi}$ by interpolation as

$$\hat{\Phi}(x, p) = h(X_0, Z_0, x, p), \quad (58)$$

where h is an interpolation method with parameters p , e.g., the K-Nearest Neighbours (k-NN). The question is how to choose the parameters p ? One way would be to simply evaluate the lifting error across all datapoints and select the best one as

$$p^* = \operatorname{argmin}_{p \in P} \sum_{x \in X_0} \|g(x) - C\hat{\Phi}(x, p)\|_Q^2, \quad (59)$$

where P is the parameter space. We use the $\|\cdot\|_Q$ norm to make the weighting consistent with the KMPC cost function in (54). Another possibility is to adapt the interpolation scheme dynamically to the current initial point x_{init} of the MPC as

$$p^* = \operatorname{argmin}_{p \in P} \|g(x_{\text{init}}) - C\hat{\Phi}(x_{\text{init}}, p)\|_Q^2. \quad (60)$$

Doing this would ensure the precision of the first few steps of the prediction, as well as the precision of the first control input, which is used for the closed-loop control. The tradeoff is that every iterate of the closed-loop would involve searching for the best interpolation parameters either via solving an optimization problem, or simply by evaluating the lifting function $|P|$ times (if the search space P is finite, such as for k-NN).

6.2.4 Invertibility of Ψ

The function Ψ might be required to be invertible if we intent to use its continuous interpolation in the MPC.

In order to ensure this, we can either manually limit the domain of each channel to its invertible parts, which boils down to manually limiting the domain of n_u scalar functions of one variable.

Another option is enforcing monotonicity of individual Ψ_k by adding the following regularization as the additional cost term $\theta(\cdot)$ in (21):

$$\left\| \left| v_k^{q_k} - v_k^1 \right| - \sum_{i=1}^{q_k-1} |v_k^{i+1} - v_k^i| \right\|_2^2, \quad (61)$$

where v_k are samples of Ψ_k . The cost (61) is explained in the following Lemma.

Lemma 3. *A sequence of q_k consecutive samples $[v_k^1, \dots, v_k^{q_k}]$ is monotonous if and only if*

$$|v_k^{q_k} - v_k^1| = \sum_{i=1}^{q_k-1} |v_k^{i+1} - v_k^i|. \quad (62)$$

Proof. The final element of the sequence can be written as

$$v_k^{q_k} = v_k^1 + \sum_{i=1}^{q_k-1} \epsilon_i, \quad (63)$$

where $\epsilon_i = v_k^{i+1} - v_k^i$. We reorganize the terms

$$v_k^{q_k} - v_k^1 = \sum_{i=1}^{q_k-1} \epsilon_i \quad (64)$$

and put both sides of the equation in absolute value

$$|v_k^{q_k} - v_k^1| = \left| \sum_{i=1}^{q_k-1} \epsilon_i \right|. \quad (65)$$

If the function is monotonous, all the ϵ_i have the same sign and hence

$$\left| \sum_{i=1}^{q_k-1} \epsilon_i \right| = \sum_{i=1}^{q_k-1} |\epsilon_i|. \quad (66)$$

Finally, by assuming the monotonicity of Ψ_k , we can put (65) and (66) together and we obtain

$$|v_k^{q_k} - v_k^1| = \sum_{i=1}^{q_k-1} |\epsilon_i| = \sum_{i=1}^{q_k-1} |v_k^{i+1} - v_k^i|. \quad (67)$$

Therefore, if the sequence v_k^i is monotonous, the equality (62) must hold.

Let us now prove the other direction. We claim that if (62) holds, then the function is monotonous. In the simple cases where the terms inside the absolute values are either all non-negative or non-positive, it is trivial to see that the function will be non-decreasing or non-increasing respectively.

The interesting case is where the signs are different. Let us assume, without loss of generality, that $v^2 - v^1 \leq 0$, and all the other terms are nonnegative. If we rewrite (67) without the absolute values, we obtain

$$(v_k^1 - v_k^2) + (v_k^3 - v_k^2) + (v_k^4 - v_k^3) + \dots + (v_k^{q_k} - v_k^{q_k-1}) = v_k^{q_k} - v_k^1. \quad (68)$$

It is clear that

$$v_k^1 - v_k^2 = 0, \quad (69)$$

therefore Ψ_k will be monotonically non-decreasing. The same approach can be used for multiple sign changes, which concludes the proof. \square

7 Summary: Koopman MPC

The algorithm 2 summarizes the procedure for designing the KMPC.

Algorithm 2 Create the Koopman MPC

Input: $A, B, C, Z_0, V_k, H, Q, R, R_d$

- 1: Create interpolated lifting function $\hat{\Phi}$ according to 6.2.3.
- 2: Decide on the strategy for inverting Ψ as in 6.2.4, optionally include the cost (61) into the term $\theta(\cdot)$ in (21).
- 3: Decide on the strategy for dealing with the input rate bounds, if applicable, according to 6.2.2.
- 4: Formulate the KMPC, either in the sparse (54) or the dense (91) formulation.

Output: function $\text{KMPC}(y_{\text{ref}}, x_0, u_{\text{prev}}) \rightarrow v^*$

The algorithm 3 shows the usage of KMPC in closed loop. The step 6 is equivalent to applying the control inputs to the real system.

Algorithm 3 Closed loop KMPC usage

Input: y_{ref} , KMPC

- 1: Initialization: $u_{\text{prev}} \leftarrow 0, x_0 = x_{\text{init}}$
 - 2: **while** true **do**
 - 3: $z_0 \leftarrow \hat{\Phi}(x_0)$.
 - 4: $v_0^* \leftarrow \text{KMPC}(y_{\text{ref}}, x_0, u_{\text{prev}})$ [Problem 54]
 - 5: $u_0^* \leftarrow \hat{\Psi}^{-1}(v_0^*)$
 - 6: $x_0 \leftarrow f(x_0, u_0^*)$
 - 7: $u_{\text{prev}} \leftarrow u_0^*$
 - 8: Wait for the next timestep.
 - 9: **end while**
-

8 Numerical examples

In this section, we shall demonstrate the following properties of our approach:

1. discovering discontinuous lifting functions
2. finding exact lift even for systems with multiple equilibria
3. controlling systems with multiple equilibria
4. control of realistic, highly nonlinear systems which are difficult to control with standard methods of control.

The first two properties are demonstrated in the first example, on a system with known analytical solution. The discontinuous lifting is of particular interest, since a lot of current methods (such as EDMD and its derivatives) require the prior knowledge (or guess) of the lifting function(s) Φ . In order to find the Koopman operator using these methods, we would need to know whether its lifting functions are discontinuous (along with the particular type and location of discontinuity). This is not required by our method.

The second example shows the control of a system with multiple equilibria, using the KMPC. We also use this example to demonstrate the different lifting approaches mentioned in the Section 6.2.3.

The last example is of a more practical nature; it shows that our approach can be used to stabilize a vehicle from an unstable state, and as well as to bring it into understeering drift. Vehicles are highly nonlinear systems, especially when the wheels lose grip with the road. Therefore such maneuvers are rather challenging, since they require exploitation of the nonlinear dynamics of the vehicle. We compare both maneuvers against MPC based on local linearization (LMPC).

8.1 Discontinuous lifting with multiple equilibria

This example demonstrates that our algorithm can find discontinuous lifting functions and systems with multiple equilibria. We will use the system from [30], to which the analytical solution is known. We empirically show that our algorithm converges to the analytical solution from any initial condition of the ADAM solver.

Consider the nonlinear system

$$\begin{aligned} \dot{x} &= f(x) \\ f(x) &= \begin{cases} -(x-1) & \text{if } x > 0 \\ 0 & \text{if } x = 0 \\ -(x+1) & \text{if } x < 0 \end{cases} \end{aligned} \tag{70}$$

The corresponding Koopman operator derived in [30] is of the form

$$\dot{z} = Az, y = Cz, \quad (71)$$

where

$$A = \begin{bmatrix} -1 & 1 \\ 0 & 0 \end{bmatrix} \quad (72)$$

$$C = [1 \quad 1].$$

The output $y = z_1 + z_2$ is equal to the nonlinear state x . The eigenvalues and eigenfunctions of the operator (72) are

$$\begin{aligned} \lambda_1 &= -1, & \Phi_1 &= x - \text{sign}(x), \\ \lambda_2 &= 0, & \Phi_2 &= \text{sign}(x). \end{aligned} \quad (73)$$

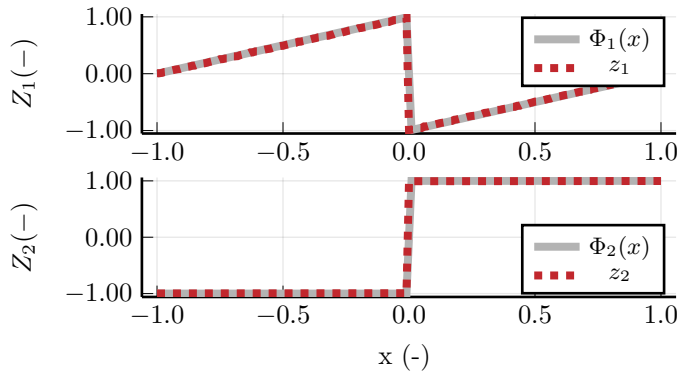


Figure 6: Comparison of analytical and learned lifted function of the one-dimensional system with multiple isolated points. We use z_1 and z_2 to denote the first and second coordinate of the lifted space.

In order to learn the Koopman predictor, we have generated 300 trajectories of the system (70) of length $H_T = 20$ which were sampled with $T_s = 0.1s$. Using the approach 1, we obtained a discrete-time Koopman predictor (\hat{A}_d, \hat{C}_d) , which was transformed into a continuous system by $(\hat{A}, \hat{C}) = (\frac{\log(\hat{A}_d)}{T_s}, \hat{C}_d)$. To compare our result with the analytical solution (72), we transformed both the analytical system (A, C) and the learned approximation (\hat{A}, \hat{C}) into observer canonical form

$$A_o = \begin{bmatrix} 0 & 1 \\ 0 & -1 \end{bmatrix}, \quad C_o = [1 \quad 0],$$

$$\hat{A}_o = \begin{bmatrix} -0.0003 & 1.0508 \\ 0.005 & -0.9989 \end{bmatrix}, \hat{C}_o = [1 \quad 0].$$

We can see that the approximated system is numerically close to the analytical solution. The continuous eigenvalues of learned Koopman system were $\hat{\lambda}_{1,2} = [-1.004 \quad 0.005]$. The estimated eigenfunctions are compared to the real ones in Fig.6.

We compare the open-loop prediction capabilities of our method with EDMD of different orders n_z in Fig.7. The basis functions for the EDMD were thin plate spline radial basis functions

$$\Phi_{\text{rbf}}(x) = \|x - x_c\|^2 \log(\|x - x_c\|), \quad (74)$$

with centers x_c selected randomly from the interval $[-1, 1]$. We can see that the proposed method provides more precision than EDMD while having only two lifted states.

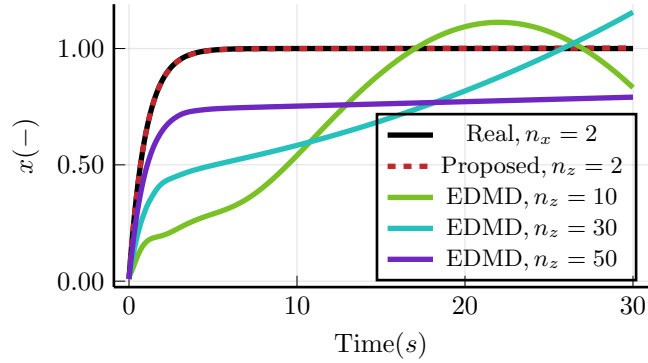


Figure 7: Open-loop predictions of our method and EDMD of different orders. The initial state of the trajectories was $x_0 = 0.01$, close to the unstable equilibrium at $x_e = 0$. The proposed predictor has the lowest order and the highest precision due to the precise identification of the discontinuous lifting functions.

To test convergence of our algorithm, we learned 100 Koopman predictors with different initial conditions of the ADAM solver generated according to 1. The eigenvalues converged to the analytical result in all cases. The results can be seen in Fig.8.

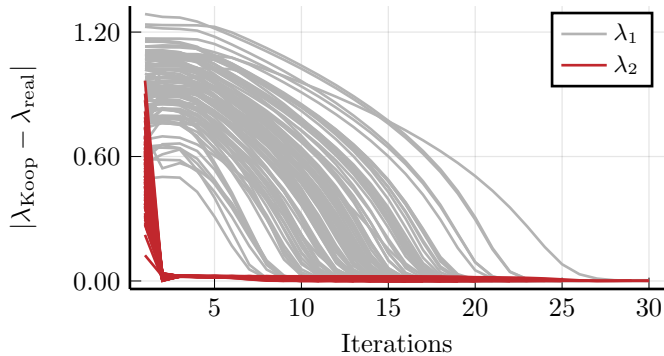


Figure 8: Evolution of the error of the continuous Koopman eigenvalues during the solver iterations for 100 different initial conditions. Since the optimization is always done in discrete time, the errors were also calculated for the discrete eigenvalues.

We can see that our approach was able to discover discontinuous eigenfunctions and system with multiple equilibria without any prior information.

8.2 Control of a system with multiple equilibria

In this example, we deal with the damped Duffing oscillator with forcing. We will show that we can steer the system into all of its equilibria, including the unstable one, with the KMPC, and compare different options for the parametrization of the interpolation method.

The continuous dynamics are

$$\begin{aligned}\dot{x}_1 &= x_2, \\ \dot{x}_2 &= -0.5x_2 - x_1(4x_1^2 - 1) + 0.5u,\end{aligned}\tag{75}$$

where $x \in [-1, 1]^2$ and $u \in [-1, 1]$. The system has 3 equilibria $x_{e_1} = [-0.5, 0]$, $x_{e_2} = [0, 0]$, and $x_{e_3} = [0.5, 0]$.

For training, we discretize the system (75) using Runge-Kutta 4 with sampling time $T_s = 0.02$ s. We used $N = 100$ trajectories, each containing 1000 samples. The trajectories were split into shorter ones with length $H_T = 20$. The lifted space has size $n_z = 30$ and the input was quantized equidistantly with 11 quantization levels.

The MPC parameters were $Q = \text{Diag}(10, 0.1)$, $R = 1$, and $H = 40$ (0.8s), $y_{[\text{up}, \text{low}]} = \pm[1, 1]$. The lifted input bounds were $\Delta v_{[\text{up}, \text{low}]} = \pm 5$, $v_{[\text{up}, \text{low}]} = [0.108, -0.11]$. Note that the values of the lifted space variables depend on the initial conditions of the ADAM solver. The results of the closed-loop simulations of the MPC controller can be seen in Figure 9.

As mentioned before, this example also serves for comparison of various interpolation approaches of the lifting function Φ , discussed in Sec.6.2.3. For the interpolation method h , we select k-NN where the only parameter is the number of neighbours, here denoted as p . We compared 3 parametrization choices, listed in Table 2. All three options are compared in Fig.9. The difference between

Name	Description
1-NN	p kept at constant value 1 (snap to closest member of X_0)
p^* -NN	p kept at optimal constant value according to (59).
$p(t)$ -NN	p changed dynamically according to (60).

Table 2: Tested interpolation methods

the methods is best seen in Fig.9a, where one observes that having no interpolation might make the closed-loop unstable. Both the p^* -NN and $p(t)$ -NN methods result in stabilizing controllers, although the $p(t)$ -NN has smaller overshoots and the trajectory is smoother, especially for the state x_2 .

We also compared the closed-loop behaviour with and without the compensation of the lifting error, defined in (56). We can see in the Fig.9b that compensating for the lifting error improves all of the lifting methods, although 1-NN results in unstable closed loop when going to the third equilibrium.

The results are summarized in the Table 3 and compared by their closed-loop costs calculated as

$$J_{\text{CL}} = \sum_{t=1}^{H_{\text{CL}}} (y_{\text{ref},k} - y_t)^\top Q (y_{\text{ref},k} - y_t) + \Delta v_k^\top R \Delta v_t,\tag{76}$$

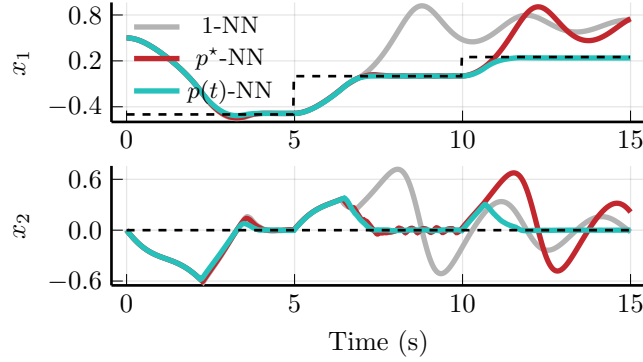
where H_{CL} is the length of a trajectory y_t with inputs v_t .

From a practical point of view, p^* -NN with lifting error compensation is a good choice, due to its low cost and low number of $\hat{\Phi}$ evaluations per iteration.

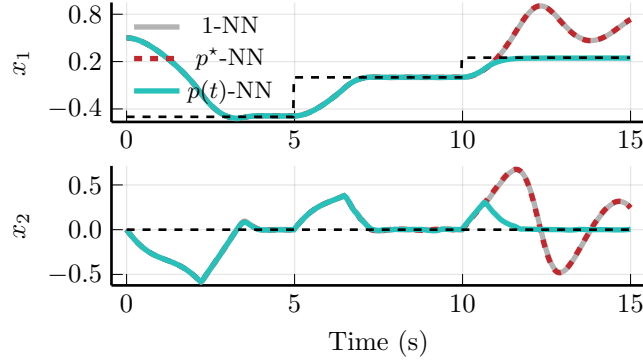
It should be pointed out that the lifting error compensation (56) is usable (and beneficial) for any Koopman-based MPC algorithm, not just our particular approach.

J_{CL}	Interpolation	Lifting compensation	Evaluations of $\hat{\Phi}$
1793.7	1-NN	no	1
1140.6	p^* -NN	no	1
794.1	$p(t)$ -NN	no	$\leq P $
1127.1	1-NN	yes	2
1123.0	p^* -NN	yes	2
793.3	$p(t)$ -NN	yes	$\leq P $

Table 3: Comparison of interpolation methods and lifting error compensation on the Duffing oscillator.



(a) Without initial-state lifting error compensation, $d = 0$.



(b) With constant initial-state lifting error compensation, d according to (56).

Figure 9: Comparison of various interpolation methods on the Duffing oscillator. The legend is explained in the Table 2. The figure 9a is without lifting error compensation. The black dashed line is the reference system.

8.3 Singletrack vehicle model

This example will show the algorithm on a singletrack vehicle model used in [18]. We shall present open-loop prediction capabilities, show that the lifted variables may have real-world physical meaning, and demonstrate the advantage of using the KMPC over a local-linearization-based MPC (we shall call it Linear MPC from now on).

8.3.1 Model description

Due to the complex nature of the model, we shall present it only as a black-box model and refer the reader to [18, Section 2] for full model derivation.

The vehicle is modeled as a planar singletrack model, also referred to as bicycle model. The main source of nonlinearities are the tires, which are modeled using the high-fidelity "Pacejka tire model (2012)". This tire model contains over a hundred of parameters, which are measured on the physical tire itself. The parameter set used in this work is from the *Automotive Challenge 2018* organized by Rimac Automobili. We refer the reader to [31, Chapter 4] for details on the full tire model.

For our purposes, the vehicle is a nonlinear function

$$\begin{bmatrix} \dot{v}_x \\ \dot{v}_y \\ \dot{r} \end{bmatrix} = f_v \left(\begin{bmatrix} v_x \\ v_y \\ r \end{bmatrix}, \begin{bmatrix} \delta \\ \lambda \end{bmatrix} \right), \quad (77)$$

where the states v_x (m/s), v_y (m/s), and r (rad/s) are the vehicle longitudinal, lateral, and angular velocities in this order. The inputs δ (°) and λ (-) are the front steering angle and the rear-tire slip ratio respectively. The bounds on the states and inputs are $v_x \in [0, 30]$ m/s, $v_y \in [-30, 30]$ m/s, $r \in [-15, 15]$ rad/s, $\delta \in [-30, 30]^\circ$, and $\lambda \in [-1, 1]$.

The model was discretized using Runge-Kutta 4 with sample time $T_s = 0.02s$.

8.3.2 Dataset design

The number of learning trajectories was $N = 8384$ with length $H_T = 10$ (0.2s). A state was considered feasible if its kinetic energy was less than 300kJ, forward velocity v_x was positive, and the front-wheel slip angles were less than 15° . A trajectory was considered feasible if 70% of its states were feasible.

8.3.3 Analysis of the Koopman predictor

Before presenting results of closed-loop control, we would like to show properties of the approximated Koopman operator.

The open-loop predictions remain accurate far longer than the $H_T = 10$ used for learning. The Figures 10 and 11 show trajectories of length $H_{ol} = 100$; the former uses a state from Z_0 as an initial condition, whereas the latter uses a state with non-negligible lifting error. Both examples show good prediction and asymptotic properties, considering the fact that they are 10 times longer than the learning trajectories.

Another notable result are the lifting functions in the Figures 12 and 13: they appear to have a physical meaning. The lifting function of the steering angle (Fig.12) has a shape of a lateral force characteristics under constant acceleration, and the lifting function of the rear slip ratio (Fig.13) has the typical shape of a longitudinal force characteristics. This means that both lifted inputs can be thought of as scaled and shifted forces, which are a major nonlinearity present in the vehicle model.

8.3.4 Control

In this section, we compare the KMPC against Linear MPC on the test cases presented in our previous work [18]. The operating point of the Linear MPC is $x_{op} = [16.7 \ 0 \ 0]^\top$, $u_{op} = [0 \ 0]^\top$

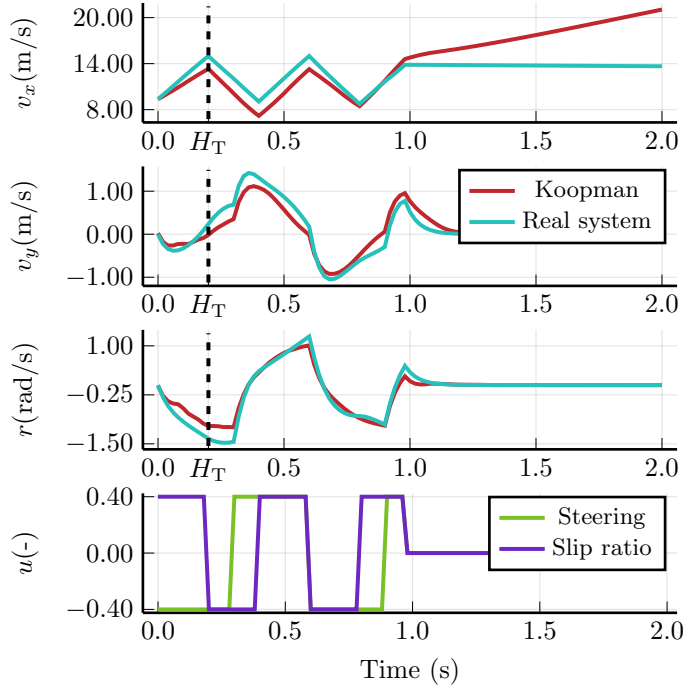


Figure 10: Open-loop prediction with square-wave forcing. The inputs are normalized. The black dashed line shows the learning horizon H_T . The trajectory is 10 times longer than the learning trajectories \mathcal{T}_i . The initial state is taken from the set Z_0 used for learning. The second half of the trajectory shows the asymptotic properties of the predictor; the longitudinal velocity slowly increases, we attribute this to the fact that the predictor is always actuated in the lifted state space (see Fig.13).

unless said otherwise.

We show that the KMPC is able to control the vehicle during standard maneuvers as well as stabilize the vehicle from nonlinear states with loss of traction.

The MPC parameters were $Q = \text{Diag}(0.01, 1, 100)$, $R_v = \text{Diag}(300, 30)$, and $H = 30$ (0.6s). The bounds on outputs and inputs were set according to the model description (77).

The input rate constraints were not used in neither of the two controllers in order to make them comparable. The Linear MPC had the same parametrization as KMPC, except for the input-weighting matrix R_u , which was calculated by scaling R_v as

$$R_u = R_v \odot s s^\top, \quad (78)$$

where \odot denotes element-wise multiplication and s is a scaling vector, $s_k = (\max(V_k) - \min(V_k))/2$. The scaling was necessary to make the two controllers comparable, since KMPC optimizes the lifted input whereas LMPC optimizes the original input.

In our previous work [18], we have already presented a Koopman-based MPC for vehicle dynamics but we were not able to outperform the linear controller at all times but only in the highly nonlinear regimes. In this section, we shall present the same tests as before, except now the KMPC clearly outperforms the linear MPC.

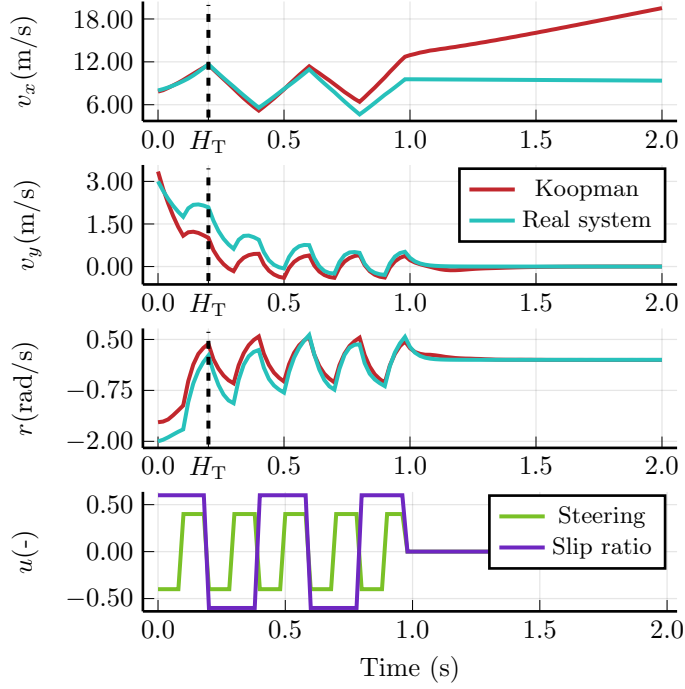


Figure 11: Open-loop prediction with square-wave forcing. The inputs are normalized. The black dashed line shows the learning horizon H_T . The trajectory is 10 times longer than the learning trajectories \mathcal{T}_i . The chosen initial state has noticeable lifting error (the trajectories starts with an offset); in spite of that, the trend of the predicted trajectory is similar to the real one. The asymptotic properties are the same as in Fig.10.

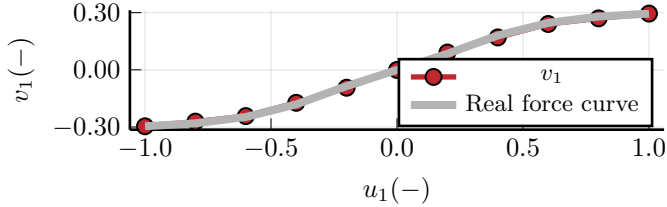


Figure 12: Lifting function of the (normalized) steering angle, compared to scaled lateral force of the front tire at $v_x = 10\text{m/s}$ with slip ratio $\lambda = 0.2$.

The first example in Fig. 14 is stabilization of the vehicle from a sideways skid. The behaviour of both controllers is the same as in [18], the only difference being is that the maneuvers are faster, due to the missing input-rate constraints.

The car starts in sideways skid $x_0 = [0 \quad -15 \quad 0]^\top$ and the goal is to perform a recovery maneuver and get the vehicle into a forward-driving state $x_{\text{ref}} = [10 \quad 0 \quad 0]^\top$. If we look at the vehicle angular

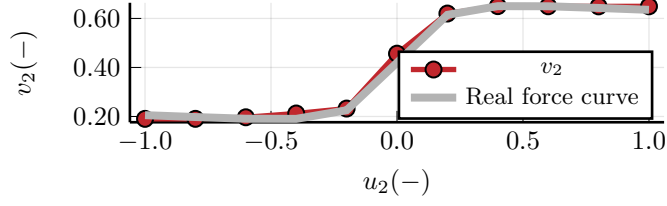


Figure 13: Lifting function of the rear slip ratio compared to a scaled and shifted real force curve of the rear tire for the vehicle driving forward at $v_x = 10\text{m/s}$. Note that the zero of the lifted input is shifted and the lifted input is always positive, we attribute this to the fact that the learning data contained mostly forward-driving states.

rate r in Fig.14, we see that the LMPC controller did opposite maneuver. The Linear MPC starts properly accelerating only when the car's angular rate is almost zero (showed by black vertical line), whereas the KMPC does both tasks at once and finishes the maneuver faster and more efficiently. As mentioned before, we refer the reader to [18, Section 6] for more detailed explanation.

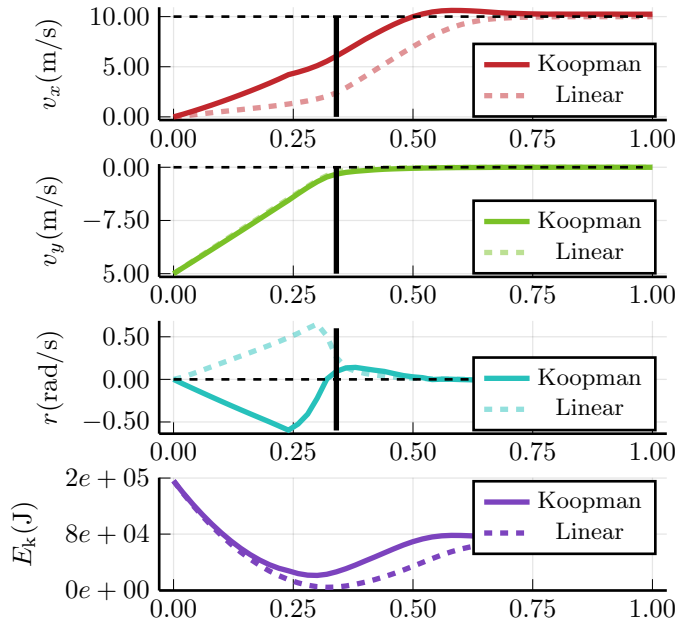


Figure 14: Stabilization of a skidding vehicle. Black dotted line is the reference. Last graph shows kinetic energy of the car for both maneuvers. We see that the Koopman-controlled system is stabilized faster and wastes less energy. The black vertical bar shows a point where vehicle no longer slips sideways; both controllers have similar values of v_y and r at this point, but the Koopman controller has preserved higher velocity due to exploitation of the nonlinear dynamics. We refer to reader to [18, Section 6] for more detailed explanation with better visual aid.

The second example presented in Fig.15 tests both controllers at vehicle traction limits; the

reference signal is a steadily increasing angular rate of the vehicle while keeping constant forward velocity. This time, the linear MPC is based on a vehicle linearized at a steady-state turn $x_{op} = [10.17 \ 0.243 \ 0.329]^T$, $u_{op} = [9.74 \ 0.001]^T$.

A real-world explanation for this maneuver is a vehicle going into a turn with decreasing radius (spiral). We show it to demonstrate that the KMPC can be used also in more 'classical' scenarios (in contrast with our results from [18]), as well as to show that the LMPC failed to keep the vehicle in steady-state when the yawrate reference reached $r_{ref} = 2.5$.

The Fig.16 shows what happens when we do not "guide" the controller by slowly changing the reference yawrate, but set it immediately to $r_{ref} = 2.4$, where the linear controller in Fig.15 was still following the reference yawrate. We see that the KMPC is able to reach the reference and stabilize the system, unlike the linear controller which oscillates.

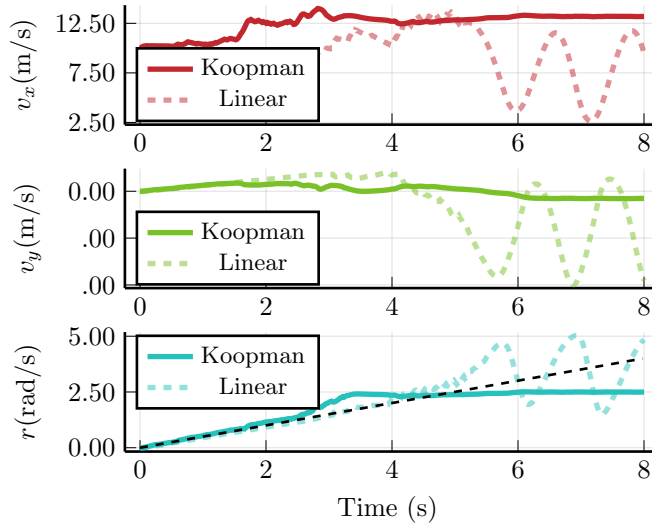


Figure 15: Left-hand turn with increasing reference yawrate amplitude.

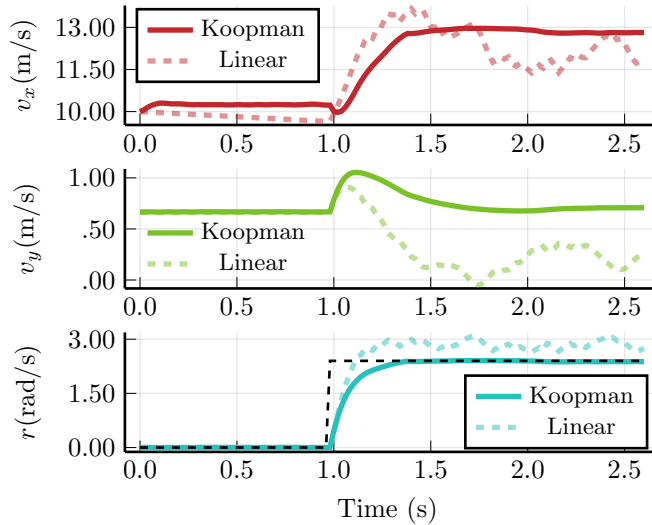


Figure 16: Sharp reference change of the yawrate r from 0 rad/s to 2.4 rad/s. Black dotted line is the reference value. The linear controller is able to get close to the reference point, but is unable to stabilize the vehicle there. The KMPC reaches the reference and stabilizes the vehicle.

9 Conclusion

We presented a novel method for learning the Koopman predictor of a controlled nonlinear dynamical system. The novelty of this approach consists in searching for both the Koopman predictor and the lifting functions at the same time, and in the transformation of the control input.

Our examples show that in the classic, autonomous setting, the approach is capable of addressing phenomena such as multiple equilibria and discontinuous lifting functions. In the controlled settings, the resulting lifting functions had a clear physical meaning, without giving the optimization routine any prior information.

We demonstrated the power of the method by bringing a vehicle model to a controlled drift, which is a maneuver that requires the exploitation of the vehicle's nonlinearities and is very difficult to do with conventional control methods.

References

- [1] B. O. Koopman, “Hamiltonian Systems and Transformation in Hilbert Space,” *Proceedings of the National Academy of Sciences*, vol. 17, no. 5, pp. 315–318, may 1931.
- [2] B. O. Koopman and J. v. Neumann, “Dynamical systems of continuous spectra,” *Proceedings of the National Academy of Sciences*, vol. 18, no. 3, pp. 255–263, 1932.
- [3] I. Mezić, “Spectral Properties of Dynamical Systems, Model Reduction and Decompositions,” *Nonlinear Dynamics*, vol. 41, no. 1-3, pp. 309–325, aug 2005.
- [4] I. Mezić and A. Banaszuk, “Comparison of systems with complex behavior,” *Physica D: Nonlinear Phenomena*, vol. 197, no. 1-2, pp. 101–133, 2004.
- [5] M. Korda and I. Mezić, “Linear predictors for nonlinear dynamical systems: Koopman operator meets model predictive control,” *Automatica*, vol. 93, pp. 149–160, jul 2018.
- [6] T. Carleman, “Application de la théorie des équations intégrales linéaires aux systèmes d’équations différentielles non linéaires,” *Acta Mathematica*, vol. 59, pp. 63–87, 1932.
- [7] A. Germani, C. Manes, and P. Palumbo, “Filtering of differential nonlinear systems via a carleman approximation approach; 44th ieee conf. on decision and control & european control conference (cdc-ecc 2005),” in *Proceedings of the 44th IEEE Conference on Decision and Control*. IEEE, 2005, pp. 5917–5922.
- [8] A. Rauh, J. Minisini, and H. Aschemann, “Carleman linearization for control and for state and disturbance estimation of nonlinear dynamical processes,” *IFAC Proceedings Volumes*, vol. 42, no. 13, pp. 455–460, 2009.
- [9] A. Armaou and A. Ataei, “Piece-wise constant predictive feedback control of nonlinear systems,” *Journal of Process Control*, vol. 24, no. 4, pp. 326–335, 2014.
- [10] A. Surana, “Koopman operator based observer synthesis for control-affine nonlinear systems,” in *2016 IEEE 55th Conference on Decision and Control (CDC)*. IEEE, 2016, pp. 6492–6499.
- [11] S. L. Brunton, M. Budišić, E. Kaiser, and J. N. Kutz, “Modern koopman theory for dynamical systems,” *SIAM Review*, vol. 64, no. 2, pp. 229–340, 2022.
- [12] H. Arbabi and I. Mezić, “Ergodic theory, dynamic mode decomposition, and computation of spectral properties of the koopman operator,” *SIAM Journal on Applied Dynamical Systems*, vol. 16, no. 4, pp. 2096–2126, 2017.
- [13] M. O. Williams, I. G. Kevrekidis, and C. W. Rowley, “A Data-Driven Approximation of the Koopman Operator: Extending Dynamic Mode Decomposition,” *Journal of Nonlinear Science*, vol. 25, no. 6, pp. 1307–1346, jun 2015.
- [14] Q. Li, F. Dietrich, E. M. Bollt, and I. G. Kevrekidis, “Extended dynamic mode decomposition with dictionary learning: A data-driven adaptive spectral decomposition of the koopman operator,” *Chaos: An Interdisciplinary Journal of Nonlinear Science*, vol. 27, no. 10, p. 103111, 2017.
- [15] M. Korda and I. Mezić, “Optimal construction of koopman eigenfunctions for prediction and control,” *IEEE Transactions on Automatic Control*, vol. 65, no. 12, pp. 5114–5129, 2020.
- [16] S. E. Otto, S. Peitz, and C. W. Rowley, “Learning bilinear models of actuated koopman generators from partially-observed trajectories,” *arXiv preprint arXiv:2209.09977*, 2022.

- [17] A. Salova, J. Emenheiser, A. Rupe, J. P. Crutchfield, and R. M. D’Souza, “Koopman operator and its approximations for systems with symmetries,” *Chaos: An Interdisciplinary Journal of Nonlinear Science*, vol. 29, no. 9, p. 093128, 2019.
- [18] V. Cibulka, M. Korda, T. Haniš, and M. Hromčík, “Model predictive control of a vehicle using koopman operator,” Mar. 2021.
- [19] M. Švec, Š. Ileš, and J. Matuško, “Model predictive control of vehicle dynamics based on the koopman operator with extended dynamic mode decomposition,” 03 2021, pp. 68–73.
- [20] —, “Predictive approach to torque vectoring based on the koopman operator,” in *2021 European Control Conference (ECC)*, 2021, pp. 1341–1346.
- [21] D. P. Kingma and J. Ba, “Adam: A method for stochastic optimization,” Dec. 2014.
- [22] M. Innes, “Flux: Elegant machine learning with julia,” *Journal of Open Source Software*, 2018.
- [23] M. Innes, E. Saba, K. Fischer, D. Gandhi, M. C. Rudilosso, N. M. Joy, T. Karmali, A. Pal, and V. Shah, “Fashionable modelling with flux,” *CoRR*, vol. abs/1811.01457, 2018. [Online]. Available: <https://arxiv.org/abs/1811.01457>
- [24] M. Innes, “Don’t unroll adjoint: Differentiating ssa-form programs,” *CoRR*, vol. abs/1810.07951, 2018. [Online]. Available: <http://arxiv.org/abs/1810.07951>
- [25] J. Bezanson, A. Edelman, S. Karpinski, and V. B. Shah, “Julia: A fresh approach to numerical computing,” *SIAM review*, vol. 59, no. 1, pp. 65–98, 2017. [Online]. Available: <https://doi.org/10.1137/141000671>
- [26] D. Mayne, J. Rawlings, C. Rao, and P. Scokaert, “Constrained model predictive control: Stability and optimality,” *Automatica*, vol. 36, no. 6, pp. 789–814, jun 2000.
- [27] A. Bambade, S. El-Kazdadi, A. Taylor, and J. Carpentier, “PROX-QP: Yet another Quadratic Programming Solver for Robotics and beyond,” in *RSS 2022 - Robotics: Science and Systems*, New York, United States, June 2022. [Online]. Available: <https://hal.inria.fr/hal-03683733>
- [28] B. Stellato, G. Banjac, P. Goulart, A. Bemporad, and S. Boyd, “OSQP: an operator splitting solver for quadratic programs,” *Mathematical Programming Computation*, vol. 12, no. 4, pp. 637–672, 2020. [Online]. Available: <https://doi.org/10.1007/s12532-020-00179-2>
- [29] M. Garstka, M. Cannon, and P. Goulart, “COSMO: A conic operator splitting method for convex conic problems,” *Journal of Optimization Theory and Applications*, vol. 190, no. 3, pp. 779–810, 2021. [Online]. Available: <https://doi.org/10.1007/s10957-021-01896-x>
- [30] C. Bakker, K. E. Nowak, and W. S. Rosenthal, “Learning koopman operators for systems with isolated critical points,” in *2019 IEEE 58th Conference on Decision and Control (CDC)*. IEEE, dec 2019.
- [31] H. Pacejka, *Tire and Vehicle Dynamics*. Elsevier LTD, Oxford, 2012. [Online]. Available: https://www.ebook.de/de/product/18341528/hans_pacejka_tire_and_vehicle_dynamics.html

[Condensed MPC formulation] In this section, we show that the problem (54) can be formulated in a way, that makes its size independent of n_z . This is very useful for the Koopman operator, since n_z will be usually large in most applications.

We restate the problem (54) for convenience

$$\begin{aligned}
\min_{\Delta v_t, z_t} \quad & \sum_{t=1}^H \|y_{\text{ref}} - y_t\|_Q^2 + \|v_t\|_R^2 + \|\Delta v_t\|_{R_d}^2 \\
\text{s.t.} \quad & z_{t+1} = Az_t + Bv_t \\
& y_t = Cz_t \\
& v_t = \Delta v_t + v_{t-1} \\
& y_{\text{low}} \leq y_t \leq y_{\text{up}} \\
& v_{\text{low}} \leq v_t \leq v_{\text{up}} \\
& \Delta v_{\text{low}} \leq \Delta v_t \leq \Delta v_{\text{up}} \\
& z_0 = \Phi(x_0) \\
& v_0 = \Psi(u_{\text{prev}}),
\end{aligned} \tag{79}$$

where $y_t = \begin{bmatrix} \hat{X}_t \\ \hat{x}_t \end{bmatrix}$, $Q \succcurlyeq 0$, $R \succcurlyeq 0$, and $R_d \succ 0$.

The output trajectory of (79) can be written as

$$\begin{bmatrix} y_1 \\ y_2 \\ \vdots \\ y_H \end{bmatrix} = \begin{bmatrix} CB & & & \\ CAB & CB & & \\ \vdots & & \ddots & \\ CA^{H-1}B & \dots & & CB \end{bmatrix} \begin{bmatrix} v_0 \\ \vdots \\ v_{H-1} \end{bmatrix} + \begin{bmatrix} CA \\ CA^2 \\ \vdots \\ CA^H \end{bmatrix} z_0 \tag{80}$$

or in short as

$$Y = MV + C_z. \tag{81}$$

We see that the size of the matrix M is of size $Hn_y \times Hn_v$ and does not depend on n_z .

The input rates can be obtained as

$$\begin{bmatrix} \Delta v_0 \\ \Delta v_1 \\ \vdots \\ \Delta v_{H-1} \end{bmatrix} = \begin{bmatrix} I & & & \\ -I & I & & \\ & \ddots & \ddots & \\ \dots & 0 & -I & I \end{bmatrix} \begin{bmatrix} v_0 \\ v_1 \\ \vdots \\ v_{H-1} \end{bmatrix} + \begin{bmatrix} -I \\ 0 \\ \vdots \\ 0 \end{bmatrix} v_{\text{prev}} \tag{82}$$

or in short as

$$\Delta V = DV + C_v \tag{83}$$

The first term in the cost function can be rewritten as

$$\begin{aligned}
\sum_{t=1}^H \|y_{\text{ref}} - y_t\|_Q^2 &= (Y - Y_{\text{ref}})^\top Q_H (Y - Y_{\text{ref}}) \\
&= Y^\top Q_H Y - 2Y_{\text{ref}}^\top Q_H Y + Y_{\text{ref}}^\top Q_H Y_{\text{ref}} \\
&= V^\top (M^\top Q_H M) V - 2(C_z - Y_{\text{ref}})^\top Q_H M V + C_0
\end{aligned} \tag{84}$$

where C_0 contains terms that do not depend on V and Y_{ref} is a column vector of y_{ref} repeated H -times. The second term is

$$\begin{aligned} \sum_{t=1}^H \|\Delta v_t\|_{R_d}^2 &= \Delta V^\top R_{d,H} \Delta V \\ &= V^\top (D^\top R_{d,H} D) V + 2C_v^\top R_{d,H} D V + C_1, \end{aligned} \quad (85)$$

where C_1 is a term that does not depend on V .

Finally

$$\sum_{t=1}^H \|v_t\|_R^2 = V^\top R_H V. \quad (86)$$

The total cost can be written as

$$V^\top F V + q^\top V, \quad (87)$$

where

$$F = M^\top Q_H M + D^\top R_{d,H} D + R_{d,H} \quad (88)$$

and

$$q = (-2(C_z - Y_{\text{ref}})^\top Q_H M + 2C_v^\top R D)^\top. \quad (89)$$

The constraints can be written as

$$\begin{bmatrix} M \\ -M \\ I_{H \cdot n_v} \\ -I_{H \cdot n_v} \\ D \\ -D \end{bmatrix} V + \begin{bmatrix} C_z \\ -C_z \\ 0 \\ 0 \\ C_v \\ -C_v \end{bmatrix} \leq \begin{bmatrix} y_{\text{up}} \\ -y_{\text{low}} \\ v_{\text{up}} \\ -v_{\text{low}} \\ \Delta v_{\text{up}} \\ -\Delta v_{\text{low}} \end{bmatrix} \quad (90)$$

or in short as $HV + H_0 \leq h$.

With the formulas (88),(89), and (90) we can write (79) as the following QP

$$\begin{aligned} \min_V \quad & V^\top F V + q^\top V \\ \text{s.t.} \quad & HV + H_0 \leq h. \end{aligned} \quad (91)$$